PCCP

Accepted Manuscript

ROYAL SOCIETY OF CHEMISTRY

www.rsc.org/pccp

Sonochemical approach improves the CuO-ZnO/TiO_2 catalyst for WGS reaction

Nina Perkas[a], Poernomo Gunawan[b], Galina Amirian[a], Zhan Wang[b], Ziyi Zhong[*b] and Aharon Gedanken[*a]

[a]*Department of Chemistry at Bar-Ilan University Center for Advanced Materials and Nanotechnology, Bar-Ilan University Center for Advanced Materials and Nanotechnology, Ramat-Gan 52900, Israel;*
[b]*Institute of Chemical and Engineering Sciences, 1 Pesek Road, Jurong Island, Singapore 627833, Singapore*

The CuO-ZnO composite was deposited onto two kinds of titania supports, which are synthetic mesoporous TiO_2 and commercial TiO_2 P25 (Degussa), *via* the ultrasound assisted precipitation and incipient wetness impregnation (IWI) methods, respectively. The catalysts were tested for WGS reaction in the temperature range of 200-400 ^oC, and the best catalytic performance was achieved on the sonochemically prepared catalysts supported on the commercial TiO_2 P25, which contains well crystallized anatase and rutile phases. Although the synthetic mesoporous TiO_2 has a higher surface area, its textural structure is not stable under the reaction conditions that leads to gradual deactivation of the CuO-ZnO/TiO_2 catalyst. It is found that the sonochemical preparation offers at least two advantages: (1) generation of mesopores on the catalyst surface and (2) doping of ZnO into CuO phase. The doping of ZnO, particularly in the case of commercial TiO_2 P25, provides high activity and extra stability to the active phase of Cu^0. These new findings provide new insights to the design and development of better heterogeneous catalysts for WGS reaction.

Keywords: mesoporous materials, nanoparticles, oxides, ultrasound

Corresponding authors: Aharon.Gedanken@biu.ac.il and Zhong_ziyi@ices.a-star.edu.sg

1 Introduction

The CuO-ZnO combination is the main component of the industrially important catalysts for methanol synthesis[1,2] and WGS reaction.[3-5] The WGS process is used to convert CO and H_2O to H_2 and CO_2 products. This reaction is exothermic (ΔH = - 41kJ/mol), which is equilibrium limited at high temperatures, and kinetically limited at low temperatures. Commercially, a combination of two catalysts, which work at high temperature (HT) and low temperature (LT) ranges respectively, is applied. The industrial HT WGS reaction usually uses the Fe_2O_3-Cr_2O_3 catalyst, while the LT WGS reaction is performed with the $Cu/ZnO/Al_2O_3$ catalyst.[6,7]

For effective application in fuel cells or in ammonia production, high purity H_2 is necessary, which means that amount of carbon oxides, in particular CO, must be reduced to very low levels. The extent of CO conversion is limited by chemical equilibrium in the reformer system, which is the major industrial process to produce syngas and hydrogen from hydrocarbons. The Cu-type catalysts are often used in the WGS reaction in the low temperature range of 200–300°C, but their catalytic activity drops quite fast. In addition, copper is more susceptible to thermal sintering, whereas the addition of ZnO stabilizes the copper component structurally.[6] The detailed structure-property of this type of catalysts is still not fully understood, particularly for the industrial catalysts under the reaction conditions. Furthermore, it is still possible to further improve the catalysts performance by controlling their microscopic structure *via* more effective catalyst preparation. For example, it is reported that the less active Cu/ZnO catalysts comprise a heterogeneous mixture of large and isolated Cu and ZnO particles, while the more active

catalysts show small and homogeneously mixed Cu and ZnO particles.[8] The development of more efficient catalysts will not only increase the reaction rate at low temperatures, but also reduce the volume of the reformer system.[6,9,10] Therefore, it is still of great interest to improve the Cu-based catalysts for the WGS reaction.

It is reported that the deposition of Cu and Au nanoparticles on TiO_2(110) crystal generates promising catalysts for the WGS reaction, with Au component often leads to lower reaction temperatures.[11] However, it seems that the Cu-based catalyst still has advantages over Au-based catalysts in this reaction, because Cu nanoparticles can preferentially bind to the terrace and steps of the TiO_2(110) surface, which would not only affect the growth mode of the surface cluster, but also enhance the catalytic activity, whereas Au nanoparticles favors the surface vacancies, resulting in poorer catalytic performance than that of Cu.[11,12]

Despite the studies of multi-component Cu catalysts, including the commercial Cu-ZnO/Al_2O_3, there has been limited information on CuO-ZnO/TiO_2 composition available in the literature. It is supposed that the CuO-ZnO/TiO_2 catalyst may combine the catalytic activity of copper with functions of ZnO against sintering and sulfur poisoning as well as the "redox" ability of TiO_2.

In the present work, we report the synthesis and catalytic properties of CuO-ZnO/TiO_2 in WGS reaction. Previously, we have demonstrated that the sonochemical method, which is environmentally benign as compared to most of the catalyst preparation methods, is able to prepare highly dispersed supported catalysts,[13-15] and very recently, we have proven that, with the same method, Zn^{2+} could be doped into the CuO lattice.[16] We thus have applied the sonochemical method to deposit CuO-ZnO composite onto the

mesoporous and commercial TiO_2 by a one-step process. As observed, an improved catalytic activity and stability are obtained for the sonochemically prepared CuO-ZnO/TiO_2 catalysts than those prepared by the IWI method, showing that the sonochemical approach is able to generate a more homogeneous structure that is important for the WGS reaction. In addition, the structure and morphology of the catalysts have been characterized by X-ray diffraction (XRD), temperature-programmed reduction (TPR), transmission electron microscopy (TEM), N_2 isothermal adsorption/desorption (BET), and X-ray photoelectron spectroscopy (XPS), so that an insight into the structure-property relationship is obtained.

2 Experimental

2.1 Catalysts preparation

All the reagents were of analytical grade and purchased from Sigma-Aldrich unless specifically mentioned. Mesoporous TiO_2 (MSP) was prepared by an ultrasound-assisted method described elsewhere.[17] Before the deposition of the CuO-ZnO active component, the TiO_2 (MSP) support was heated at 400 ^oC for 2 h or at 500 ^oC for 3 h, while the commercial TiO_2 P25 (Degussa) was used as purchased.

The sonochemical deposition procedures were as follows: 2.81g Cu (II) acetate and 1.03g Zn (II) acetate with a molar ratio of Cu/Zn=3/1 were dissolved in 25 ml of distilled water and mixed with 225 ml ethanol (volume ratio of water/ethanol = 1/9). The TiO_2 powder (0.5g) was added to the reagents solution to get the molar ratio of (Cu+Zn)/Ti as 3/1. The reaction slurry was exposed to sonication for 2 h using an immersed Ti horn (20 kHz, 100 W/cm^2 at 60% efficiency). The pH value of the working

solution was adjusted to 8 with 25 wt% aqueous solution of ammonia added dropwise during the reaction to ensure the hydrolysis of the copper and zinc salts. The product was then separated by centrifugation, washed three times with ethanol and dried in vacuum overnight. For comparison, a catalyst of Cu/TiO_2 P25 was also prepared by the same method. The preparation by the IWI method was performed as follows: the same amounts of reagents and solvent as in the above preparation were dispersed thoroughly and stirred for 4 h. The excess of the solvent was evaporated in a boiling water bath. The precipitate was dried at 120 ^{o}C for 24 h. All the catalysts were calcined in a furnace at 350 ºC for 4 h at a ramp rate of 1 ºC/min, and are listed in Table 1.

2.2 Catalysts characterization

The XRD analysis was performed on a Bruker D8 diffractometer with Cu-Kα radiation. The elements content was evaluated by energy-dispersive X-ray analysis (EDX) using an Inspect FEI scanning microscope. Sample morphology and structure were studied by high resolution transmission electron microscopy (HRTEM) on Tecnai TF20 Super Twin at 200 kV. Surface area, pore volume and pore size distribution were measured using a Nova 3200e Quantachrome analyzer. The surface area was calculated from the linear part of the BET plot. Pore size distribution was estimated using the Barret–Joyner–Halenda (BJH) model with the Halsey equation, and the pore volume was measured at the P/P_0 0.9947 signal point.

Temperature programmed reduction (TPR) was conducted on a Thermo TPDRO 110 catalyst analyzer system. The conditions of the experiments were as follows: 100 mg of sample was pre-treated in Ar flow of 50 cc/min at the temperature interval of 30-300 ^{o}C. The ramp rate was 10 ^{o}C/min and the sample was maintained at 300 ^{o}C for another 30

min. After cooling down to room temperature in Ar, it was switched to a gas mixture of 5% H_2-95% Ar with a flow rate of 50 cc/min. The TPR analysis was performed at the temperature interval of 30-500 ^oC with the ramp rate of 10 ^oC/min, and was maintained at 500 ^oC for another 20 min. The XPS analysis for the reacted catalysts was carried out using Thermo Scientific VG ESCALAB 250 with survey scans from 0-1100 eV and individual element scanning of O1s, Ti2p, Cu2p, and Zn2p. Prior to the XPS analysis, the samples were kept in a dry box for two weeks. Micro-Raman spectroscopy measurements were performed at room temperature using a micro-Raman spectrometer from Renishaw inVia (United Kingdom) equipped with a 514 nm laser, a CCD camera, and an optical Leica microscope. A 50x objective lens to focus the incident beam and an 1800 lines/mm grating were used. For calibration, a silicon standard was used. Raman spectra were collected at least from 10 – 15 locations on a sample. The set-up measurements provided 20 – 30 sec of exposure times and 5 accumulations in the range of 100 – 1000 cm^{-1}. The spot size of the laser was estimated to be around one micron. To avoid possible photodecomposition of the samples, Raman spectra were recorded using low excitation power of 4 – 20 mW. The data were analyzed using Renishaw Wire 3.3 software.

2.3 Catalytic testing

All catalytic tests were carried out in a fixed bed reactor equipped with a quartz tube, with the sample packed in between 2 layers of quartz wool. About 130 mg of each sample was loaded for each catalytic run. The catalysts were all pretreated in 5% H_2 at 350 ºC for 3 h, cooled down to room temperature switched to the WGS reaction gas mixture that consists of 2.08% CO + 8.07% CO_2 + 18.5% H_2 + 36% H_2O (with He as

balance gas, and the gas flow rate: 24.5 ml/min; water flow rate: 0.006 ml/min). The outlet gas was analyzed on line by a Shimadzu 14B GC equipped with both TCD and FID detectors.

3 Results and discussion

3.1 Catalytic performance

The CO conversions in the WGS reaction of the studied catalysts are shown in Fig. 1. The CuO-ZnO/TiO_2 catalysts synthesized by the sonochemical method (S500 and DS) display much higher activities than those prepared by the IWI method (IWI 400 and IWI 500). For example, at 250 ^oC, the CO conversion over S500 catalyst supported on the synthetic and 500 ^oC-calcined TiO_2 is 66%, while over DS supported on the commercial Degussa TiO_2 is 84%. Both results are much higher than that one of the respective IWI derived catalysts, which exhibits almost zero conversion at 250 ^oC. For the Cu/TiO_2 catalyst prepared by the sonochemical method on P25, the CO conversion is only ca. 10% at the same reaction temperature, indicating a significant promoting effect of ZnO.

The results obtained with the sonochemically prepared CuO-ZnO/TiO_2 catalysts (S500 and DS) are comparable or even better than that on Pt containing catalysts under similar conditions.[18,19] Meanwhile, the catalyst S400 prepared by the sonochemical method has a modest CO conversion, which is 50% at 250 ^oC.

The stabilities of the two most active catalysts are studied in the life time mode at 300 ^oC (Fig. 2), and different behaviors are observed. The CO conversion of S500, which was initially *ca.* 60%, decreases monotonously within 96 hrs, while that of the DS

catalyst remains almost stable during the same period, demonstrating a higher stability of the latter.

3.2 Structure and morphology of the catalysts

The XRD studies demonstrate various crystalline structures for the synthetic TiO_2 support treated at 400 and 500 ^oC, respectively (Fig. 3a and 3d). For the mesoporous TiO_2, after calcination at 400 ^oC, only the anatase phase is observed with main diffraction peaks at $2\theta = 25.28^o$, 37.80^o, and 48.05^o, which are assigned to reflection lines of (101), (004) and (200) (JCPDS 00-021-1272) (Fig. 3d). The additional peaks at 27.45^o, 36.09^o and 54.32^o, which are assigned to the reflection lines of (110), (101) and (211) of rutile phase (JCPDS 00-021-1276), are found only after heating of the support at 500 ^oC (Fig. 3a). There is also no change in the TiO_2 crystalline structures after the deposition procedure followed with calcination at 350 ^oC for 4h. Comparing the XRD patterns of the catalysts prepared by the sonochemical and the conventional IWI methods, it is revealed that the sonochemically prepared S500 and S400 exhibit only the copper oxide phase besides TiO_2. The peaks at $2\theta = 32.51^o$, 35.54^o, 38.73^o can be assigned to the (110), (−111), (111) diffraction lines of the monoclinic tenorite phase of CuO (JCPDS 00-041-0254). Similar XRD patterns are observed for the sonochemically prepared DS catalyst (Fig. SI-1), in which no distinct ZnO diffraction peak is observed. On the other hand, the samples IWI500 and IWI 400 synthesized by the IWI method exhibit both CuO (JCPDS 00-041-0254) and ZnO (JCPDS 00-001-1136) phases, which can be clearly distinguished. The peaks at $2\theta = 31.82^o$ and 36.50^o are assigned to (100) and (101) diffraction lines of zincite (Fig. 3b and 3e). Thus, the catalysts synthesized by IWI method present a mixture of CuO and ZnO oxides deposited on TiO_2.

The metal content in S500, DS and IWI500 catalysts has been determined by EDX analysis, and the results are shown in Fig. 4. The samples prepared by both sonochemical (S500 and DS) and conventional IWI (IWI500) methods, exhibit Cu/Ti molar ratios close to the theoretical ratio (Cu/Ti=2.25), and similar molar ratios of (Cu+Zn)/Ti as (2.6~2.8/1). At the same time, the Zn content in S500 and DS (Cu/Zn is 7.7~8/1) is lower than that in IWI500 (Cu/Zn =3/1) (Table 2). This Cu/Zn ratio is similar to the sonochemically prepared Zn-CuO composite,[16] where the single phase with Zn-doping is found to have a composition of $Cu_{0.89}Zn_{0.11}O$, which implies that out of every nine Cu^{2+} ions one is replaced by a Zn^{2+} ion in the unit cell.

All the peaks in the XRD spectra of the sonochemically prepared samples are assigned to TiO_2 or CuO. No peaks related to ZnO or any impurities were observed. However, the presence of Zn in the samples is shown in the EDX measurements. Combining the XRD and EDX results of samples S500 and DS, it can be assumed that during the sonication, the incorporation of Zn^{2+} ions into the CuO lattice takes place. The assumption on incorporation (doping) of Zn^{2+} ions into CuO lattice is based on the detailed XRD studies and calculations of the cell parameters made for the sonochemically prepared Zn-CuO nanocomposite with the same molar ratio of the components (Cu:Zn= 3:1).[16] One of the possible explanations for this phenomenon is that during the sonochemical reaction the Zn^{2+} ions replace some Cu^{2+} ions in the unit cell of the monoclinic CuO, leading to the formation of doped structure, Zn–CuO. According to the above mentioned results, we assume that the doped structure is predominant in the sonochemically prepared catalysts, whereas in the catalysts synthesized by the IWI method segregation of ZnO and CuO phases occur. It is also worth noting that in the

previous study[16] a single phase or solid solution with Zn-doping is observed only for the solution with Cu:Zn molar ratio ≥ 3:1. When more Zn precursor is introduced into the reaction (for example Cu:Zn = 1:1), distinct ZnO and CuO phases are observed in the mixture.

The morphology and the structure of S500 catalyst has been studied by TEM and the results are presented in Fig. 5. The as-prepared sample is composed of titania spheres with a dimension of 150-200 nm densely coated with smaller nanoparticles of 15-20 nm in size (Fig. 5a). The fringe analysis of the HRTEM image shows that the TiO_2 spheres consist of two phases: anatase and rutile, and the coating small particles are the tenorite phase of CuO (Fig. 5b). The separate phase of ZnO is not found, although various areas are checked, which is generally in agreement with the above XRD results. After the catalytic reaction, some nanoparticle aggregates are found deposited on the TiO_2 spheres (Fig. 5c and 5d). After 90 hours of the stability test, some rod-like structures appeared (Fig. 5e and 5f). These rod-like structures are even observed in the H_2-reduced S500 sample. A detailed HRTEM analysis for many regions in the H_2-reduced S500 sample shows that this rod-like structure is anatase, not CuO (Fig. SI-2). Hence, the degradation of the textural structure of the mesoporous TiO_2 support should be related to the poor stability of this catalyst (Fig. 2). As shown in Table SI-1, the surface area of S500 is not decreased after the reaction, and even after the life test, indicating the surface area change is not the reason for the catalyst deactivation. It is well known that for the supported Cu catalysts, the sintering of Cu particles often leads to deactivation of the catalysts.[6] In the S500 catalyst, the degradation of the mesoporous TiO_2 due to development of rod-like

TiO_2 probably will weaken the interaction of the active component with the support, and hence, makes the active component more prone to aggregation and sintering.

The TEM results also show (Fig. 6) that the DS catalyst prepared by the sonochemical method using the commercial titania as the support exhibits smaller particle size than the synthetic TiO_2 (50-100 nm), which remained almost the same particle size even after a 90h stability test. More importantly, unlike S500, no rod-like structures are observed in the DS catalyst after the H_2 reduction (Fig. SI-3) and after the life test (Fig. 6). These characteristics probably endow this catalyst with much higher catalytic stability as shown in Fig. 2. According to the XRD analysis, Degussa TiO_2 P25 used in the preparation of the DS sample has the well developed crystalline structure that can provide high stability during the catalytic reaction. Comparing the catalytic performances of S500 and S400 (Fig. 1), it suggests that the stability of TiO_2 support is important to the stability of the catalysts, although the latter has a much higher surface area than the former (Table 1).

The N_2 adsorption-desorption isotherms of the catalysts are presented in Fig. 7. The BET measurements show that all the catalysts prepared by the sonochemical method are mesoporous. For both TiO_2 supports, TiO_2-500 and TiO_2-400, the hysteresis loops are similar to those of H2 type mesopores according to the IUPAC classification. The surface area and pore volume of TiO_2-400 are 3- and 2-fold larger than those of TiO_2-500 respectively (Table 1). However, the pore size of TiO_2-400 is only 70% of that of TiO_2-500. The decrease in surface area and pore volume at elevated temperature can be attributed to the partial collapse of the pores during heating. The S500 and S400 samples display hysteresis loops similar to the corresponding titania supports, indicating

remaining of the mesoporous structure. After sonochemical deposition of the active components, the surface area of the catalysts is decreased but not drastically (Table 1). Interestingly, the pore size of the catalysts is increased compared to the bare titania supports, which is from 36 to 42 Å for S400, and from 50 to 60 Å for S500.

As it has been reported in our previous publications, the acoustic cavitation can cause the formation of mesopores and is an effective method for insertion of nanosized catalysts into the mesopores.[20.21] For the DS catalyst, which is prepared by sonochemical method using commercial TiO_2 P25 as the support, a slight increase in the surface area in comparison to the bare titania support (from 45 to 49 m^2/g) is also observed. It is accompanied with a two-fold increase of the pore volume, as well as a remarkable growth in the pores size (from <10 to 74 Å) (Table 1). All these changes in textural properties should contribute to the high catalytic activity observed for the DS catalyst. In contrast, the catalysts prepared by the conventional IWI method (IWI 500 and IWI 400) exhibit much smaller surface area, pore volume and pore size (decreased by 50-70%) after the deposition of the active components on titania. Such changes in the surface characteristics should be one reason for their low catalytic activity.

The increase in pore size after the sonochemical deposition of the active component may be due to two reasons: (i) the newly generated CuO and ZnO can stack together and form mesopores, and (ii) the acoustic cavitation causes the formation of mesopores on the TiO_2 surface, which is reported in our previous publications.[20.21] To elucidate the influence of sonochemical treatment on the texture of the titania, a control experiment has been performed with commercial TiO_2 P25 under the same sonochemical treatment conditions as for the CuO-ZnO/TiO_2 catalysts. The BET analysis has

demonstrated that after sonication, the surface area of TiO_2 P25 is slightly increased (from 45 to 52 m^2/g), while the pore volume is increased significantly (from 0.09 to 0.23 cc/g), and the pore size is enlarged by about an order of magnitude (from < 10 to 86 Å) (Table 1). The N_2 adsorption-desorption isotherm of the sonochemically treated TiO_2 clearly shows the generation of mesopores in TiO_2 P25 after sonication (Fig. SI-4). In the presence of the CuO-ZnO precursors, these newly generated mesopores are believed to be able to accommodate the formed CuO-ZnO nanoparticles. Of course, we cannot completely exclude the possibility that some of pores are formed because of the stacking of these doped CuO particles.

A possible mechanism for synthesis of the catalysts by ultrasound assisted method is presented in Scheme (Fig. 8), which illustrates how the Zn-CuO oxide particles are formed and inserted into the pores of TiO_2 support. Because of its relatively low solubility in water, copper oxide should be formed prior to the zinc oxide. The ZnO nucleus or ions will be subsequently doped into Cu oxide under the strong sonication that can not be obtained by conventional impregnation method, where the separate ZnO and CuO phases are often observed after calcination. The formed Zn doped CuO particles are further propelled to the support surface by the sonochemical micro jets with highly intensive energy, which are created in the solution as a result of the implosive collapse of the micro-bubbles in the solution.[20] Meanwhile, the sonication will generate mesopores on the catalyst support surface to accommodate the *in situ* generated Zn-CuO particles, thus making heterogeneous catalysts with the ideal microscopic structures.

3.3 Raman spectroscopy

To probe whether there is formation of $Cu_{0.89}Zn_{0.11}O$ crystal and the Zn-O-Cu exists in this structure, the Raman spectra of TiO_2-500, IWI500 and S500 were measured. The spectra are presented in Fig. 9. In all cases the clear spectrum of titania is observed. For IWI500 an additional broad feature at 440 cm^{-1} is observed, while for the sample S500, which is supposed to have a structure of $Cu_{0.89}Zn_{0.11}O$ on titania a clear peak at 300 cm^{-1} is appeared. This vibration has a close proximity to the phonons of ZnO at 275 cm^{-1} and of CuO at 292 cm^{-1}, respectively.[22-24] We assign the peak at 300 cm^{-1} to the Cu-O-Zn phonon that is slightly shifted in respect to the previous lines as a result of perturbed crystal that is obtained in the sonochemical process. It is worth mentioning that the peak at 440 cm^{-1} detected in the spectrum of IWI500 that consists of separate phases of ZnO and CuO on titania can be attributed to ZnO for which a similar peak was detected at 437 cm^{-1} in the spectrum of pristine ZnO.[22] The reason that this peak didn't appear in the spectrum of catalysts S500 is due to the lesser amount of ZnO in $Cu_{0.89}Zn_{0.11}O$ as compared to 33% in the mixture of ZnO and CuO.

3.4 TPR analysis

The TPR measurements were carried out for a number of catalysts and individual metal oxides heated at 350 ºC for 4 h. The obtained reduction peaks are de-convoluted into several sub-bands and presented in Fig.10. It can be seen that there is no any reduction peak for the mesoporous TiO_2 (the bottom line in Fig. 10), while that of the CuO is located at ca. 176^{o}C. The CuO-ZnO/TiO_2 catalyst (S500) and individual ZnO-doped CuO oxide prepared by the sonochemical method have similar reduction profiles, while the ZnO-doped CuO (without TiO_2 support) has higher reduction peaks mainly located at 236

and 258 ^{o}C respectively. These reduction peaks are de-convoluted into several sub-bands, which can be roughly divided in two groups. The 1^{sr} group has the reduction temperature below 210^{o}C, and the 2nd type - above this temperature. The reduction behavior of the DS catalyst prepared by the sonochemical method on the commercial titania (Degussa P25) demonstrates a slightly lower reduction temperature than the catalyst S500 supported on the synthesized mesoporous oxide, but in general, all the CuO-ZnO/TiO_2 catalysts display two groups of reduction peaks located both below and above 210^{o}C. The shift of the reduction temperature to higher temperature for CuO in the CuO-ZnO/TiO_2 catalysts compared with the individual CuO and TiO_2 oxides can indicate that in the studied catalysts there is a strong interaction between CuO and ZnO or TiO_2.

The reduction behaviors of our catalysts resemble those observed for CuO supported on CeO_2 and on Zn-containing hydrotalcite catalysts.[24, 25] However, it should be mentioned that, as observed by Kim et al in a series of *in situ* experiments,[26] the reduction of CuO is complex, which involves an induction period and embedding of H into the bulk of the oxide. Under a normal supply of hydrogen, CuO is reduced into metallic Cu without formation of any intermediate or suboxide (Cu_2O or Cu_4O_3).[27] Under correct reduction conditions, the reduction profiles of both CuO and Cu_2O are characterized by a single and quite sharp reduction peak, although they can also be markedly perturbed by factors such as mass transfer effect, diffusion retardation, flow rate and initial hydrogen concentration.[28,29] Considering the sufficient H_2 supply in our experiments and comparing the literature results with ours, we prefer to assign the 1st group of reduction peak below 210^{o}C to the CuO particles having a weak interaction with the catalyst support and H_2-reduction behaviors similar to that of bulk CuO, and the 2nd

group to the CuO phase with interaction with the catalyst support. The possibility for formation of Cu_2O or Cu_4O_3 in the TPR experiments should be small.[30-32]

The area ratios of the two group peaks are calculated and given in Fig.10. It seems that the catalysts (DS and S500) with high activity exhibit a medium peak area ratio of $P_1/(P_2 + P_3)$ between 0.7 –1.1, while for the catalyst with poor catalytic performance the peak area ratio is either very low or very high. Next we will focus more on the reduced catalysts, particularly on the active phase of metallic Cu in the catalysts.

3.5 XPS studies

The XPS studies were performed on the two most active S500 and DS catalysts before reaction, after reduction with H_2, after a short-term reaction, and after the 90h stability test (Fig. 11). Except from the H_2-reduced samples, the other samples were kept in a dry box for two weeks prior to the XPS measurements. The S500 catalyst displays satellite peaks before reaction, after the short-term reaction and even after the 90h life test, but the intensity ratio of the satellite peak at 942 eV to the main peak at 933 eV(Cu $2p_{3/2}$ in CuO) becomes smaller from the bottom XPS spectrum to the top one (see the calculated peak of height ratio h_2/h_1 in Fig. 11). At the same time for the DS sample the decrease in intensity of the satellite peaks looks more significant: the satellite peak is observed in the sample before reaction, but their intensity becomes much smaller after a short term reaction (the middle curve in Fig. 11, right), and is completely disappeared after a life-time reaction (the top curve in Fig. 11, right). These satellite peaks are absent in the Cu_2O and metallic Cu species.[33-35] As a comparison, we also measured the S500 and DS samples right after reduction with H_2. Although there are still two small satellite peaks

due to oxidation during the sample transfer, their intensity iss very weak indicating the active phase of the WGS reaction is metallic Cu^0, not the other phases. The binding energy of Cu_{2p} also experiences different changes for both catalysts. For S500, there is little change in the binding energy (at 933.0 eV assigned to Cu $2p_{3/2}$ in CuO) before reaction, after the reaction and after the 90h life test. On the other hand, the DS catalyst shows that the Cu_{2P} binding energy shifts *ca.* 0.5 eV from 933.2 eV (before reaction) to 932.7 eV (after the reaction), and further to 932.2 eV (after the 90h life test), indicating that reduction of copper from Cu^{2+} to Cu^{1+} or to Cu^0 occurred. Therefore, it seems that the Cu_2O phase and Cu^0 are the predominant phases on the surface of the reacted DS catalyst, but not on the reacted S500 catalyst. Keeping in mind that the catalysts were reduced at 350 ^oC in 5% H_2 prior to the reaction, the CuO phase should be completely reduced to Cu^0 according to the TPR (Fig. 10) and XPS analysis. It is well known that Cu^0 is the crucial part of the active sites. However, it should also be noted that the two catalysts were not measured immediately after the catalytic reaction, but were on hold for two weeks before the XPS analysis. During this period and the catalyst transfer, the Cu^0 and Cu_2O would have been re-oxidized. Clearly, the XPS results show that in the DS catalyst the active phase of Cu^0 is much more stable than in S500, which may explain their superior catalytic activity (Fig. 1) and stability of DS to that of S500.

3.6. Micro-structure of the DS catalyst after reduction and the role of ZnO

As found in the above experiments, there is no strong correlation between the reduction behaviors with the catalytic performances. In contrast, in DS, a much enhanced stability of metallic Cu is observed via XPS analysis, indicating that in the active catalysts the

stability of metallic Cu is crucial, which is in agreement with most of literature results. El-shobaky et al [36] reported that in CuO-ZnO/Al_2O_3 catalysts, ZnO acts as a suitable stabilizer via coating some of CuO crystallites and hindering their growth. Ressler et al [8] observed by TEM that, in the active Cu/ZnO catalysts, the small Cu particles were intimately contacted with ZnO particles, while in the less active catalysts of Cu/ZnO, large and isolated Cu and ZnO particles were identified. Density functional theory (DFT) calculations showed that in methanol and WGS atmospheres, CuCO and Cu_2HCOO species are dominated on the Cu/ZnO catalyst surface, and the transport of these species, particularly the CuCO species is responsible for the Ostwald ripening of Cu particles.[37] In our case, the Zn-CuO composite particles are sitting on the TiO_2 surface after the sonication assisted deposition (Fig.SI-3). With reduction of CuO, the doped ZnO should segregate from metallic Cu phase and form patches of ZnO that will have an intimate contact with Cu, which may enhance the activity and stability of the catalysts. To confirm this, we checked the H_2-reduced DS sample by H_2 and identified some areas that have close contact between ZnO and Cu (Fig.12). It should be pointed out that, some areas with very thin coating of ZnO may still not be identified by TEM clearly. As reported in literature, oxide-on-metal inverse catalysts can provide extra oxide-metal-interfaces that can stabilize the metal active sites.[38, 39]

4 Conclusion

In summary, both the synthetic synthesized mesoporous TiO_2, and the commercial TiO_2 P25 (Degussa) are selected as the catalyst supports for the CuO-ZnO/TiO_2 catalysts. The

deposition of the CuZnO composite and mixed cooper and zinc oxides onto TiO_2 supports is performed *via* sonochemical and IWI methods respectively. The prepared catalysts are evaluated for WGS reaction. Higher catalytic activity for WGS reaction is observed on the sonochemically prepared catalysts compared to those ones produced by the conventional IWI method. It is found that mesopores are generated in the titania during the sonochemical deposition to house the *in situ* formed Zn-doped CuO nanoparticles. Moreover, TiO_2 P25 is found superior to the synthesized mesoporous TiO_2 in terms of stability, as the textural structure of the latter is not stable under the reaction atmosphere, thus providing poorer protection to the active phase of Cu^0. For the first time it is found that doping of Zn^{2+} into CuO in the CuO-ZnO/TiO_2 catalyst by the sonochemical approach can significantly improve its catalytic performances in the WGS reaction.

References

1 G. Prieto, J. Zečević, H. Friedrich, K. P. de Jong, E. P. de Jongh, *Nature Mater.,* 2013*,* **12***,* 34-39.

2 P. Mierczynski, T. P. Maniecki, K. Chalupka, W. Maniukiewicz, W. K. Jozwiak, *Catal. Today,* 2011, **176,** 21-27.

3 R. K. Pati, I. Lee, D. Chu, S. H. Ehrman, *Prepr. Pap.- Am. Chem. Soc., Div. Fuel Chem*., 2003, **48**, 812-813.

4 P. Guo, L. Chen, G. Yu, Y. Zhu, M. Qiao, H. Xu, K. Fan, *Catal. Commun.***,** 2009, **10**, 1252–1256.

5 X. Liu, P. Guo, S. Xie, Y. Pei, M. Qiao, K. Fan, *Int. J. Hydrogen Energy,* 2012, **37,** 6381-6388.

6 R. J. Byron Smith, M. Loganathan, M. S. Shantha,. *Int. J. Chem. React. Eng.*, 2010, **8,** 1-32.

7 P. Guo, L. Chen, Q. Yang, M. Qiao, Hu. Li, He. Li, H. Xu, K. Fan, *Int. J. Hydrogen Energy*, 2009, **34**, 2361-2368.

8 T. Ressler, B. L. Kniep, I. Kasatkin, R. Schlogl, *Angew. Chem. Int. Ed.*, 2005, **44**, 4704 –4707.

9 Y. Tanaka, T. Utaka, R. Kikuchi, K. Sasaki, K. Eguchi,. *Appl. Catal. A,* 2002, **238**,

11-18.
10 N. Schumacher, A. Boisen, S. Dahl, A. A. Gokhale, S. Kandoi, L. C. Grabow, J. A. Dumesic, M. Mavrikakis, I. Chorkendorff, *J. Catal*., 2005, **229,** 265–275.
11 J. A. Rodrıguez, J. Evans, J. Graciani, J. B. Park, P. Liu, J. Hrbek, L. F. Sanz, *J. Phys. Chem. C,* 2009, **113**, 7364-7370.
12 S. F. Peng, J. J. Ho, *Phys. Chem. Chem. Phys.*, 2011, **45**, 20393-20400.
13 N. Perkas, Z. Zhong, J. Grinblat, A. Gedanken, *Catal. Lett*., 2008, **120**, 19-24.
14 N. Perkas, G. Amirian, Z. Zhong, J. Teo, Y. Gofer, A. Gedanken, *Catal. Lett.*, 2009, **130**, 455–462.
15 N. Perkas, J. Teo, S. Shen, Z. Wang, J. Highfield, Z. Zhong, A. Gedanken, *Phys. Chem. Chem. Phys.,* 2011, **13**, 15690-15698.
16 E. Malka, I. Perelshtein, A. Lipovsky, Y. Shalom, L. Naparstek, N. Perkas, T. Patick, R. Lubart, Y. Nitzan, E. Banin, A. Gedanken, *Small*, 2013, 9, 23, 4069-4076.
17 Y. Wang, X. Tang, L. Yin, W. Huang, Y. R. Hacohen, A. Gedanken, *Adv.Mater*., 2000, **12**, 1183-1185.
18 H. Iida, A. Igarashi, *Appl. Catal. A,* 2006, **298**, 152–160.
19 A. Boisen, T. V. W. Janssens, N. Schumacher, I. Chorkendorff, S. Dahl, *J. Mol. Catal. A,* 2010, **315**, 163–170.
20 A. Gedanken, X. Tang, Y. Wang, N. Perkas, Y. Koltypin, M. V. Landau, L. Vradman, M. Herskowitz, *Chem. Eur. J.*, 2001, **7**, 4546-4552.
21 M. Sivakumar, A. Gedanken, Z. Zhong, L. Chen, *New J. Chem*., 2006, **30**, 102-107.
22 K. Senthil, Y Tak, M. Seol, K. Yong, *Nanoscale Res. Lett.*, 2009, **4**, 1329–1334.
23 W. Wang, Q. Zhou, X. Fei, Y, He, P. Zhang, G. Zhang, L. Peng, W. Xie, *Cryst. Eng. Comm.,* 2010, **12**, 2232–2237.
24 B.C. Lin, S.Y. Chen, P. Shen1, *Nanoscale Res. Let*., 2012, **7,** 272-282.
25 S. Pradhan, A. S. Reddy, R. N. Devi, S. Chilukuri, *Catal. Today*, 2009, **141**, 72–76.
26 P. Gao, F. Li, F. Xiao, N. Zhao, N. Sun, W. Wei, L. Zhong, Y. Sun, *Catal. Sci. Technol.,* 2012, **2**, 1447-1454.
27 J. Y. Kim, J. A. Rodriguez, J. C. Hanson, A. I. Frenkel, P. L. Lee, *J. Am. Chem. Soc*., 2003, **125,** 10684-10692.
28 G. Fierro, M. Lo Jacono, M. Inversi, P. Porta, R. Lavecchia, F. Cioci, *J. Catal*., 1994, **148**, 709-721.
29 G. Fierro, M. Lo Jacono, M. Inversi, P. Porta, F. Cioci, R. Lavecchia, *Appl. Catal*. 1996, **137**, 327-348).
30 X. Li, S. S. Fang, J. Teo, Y. L. Foo, A. Borgna, M. Lin, Z. Zhong, *ACS Catal.* 2012, **2**, 360-369.
31 X. Zheng, X. Zhang, X. Wang, S. Wang, S. Wu, *Appl. Catal. A*, 2005, **295**, 142-149.
32 L. Li, Y. Zhan, Q. Zheng, Y. Zheng, X. Lin, D. Li, J. Zhu, *Catal. Lett*., 2007, **118**, 91–97.
33 J. A. Rodriguez, J. J. Hrbek, *Vac. Sci. Technol. A,* 1994, **12,** 2140-2144.
34 J. A. Rodriguez, J. Y. Kim, J. C. Hanson, M. Perez, M.; A. I. Frenkel, *Catal. Lett*., 2003, **85**, 247-254.
35 Z. Zhong, V. Ng, J. Z. Luo, P. Teh, J. Teo, A. Gedanken, *Langmuir*, 2007, **23**, 5971-5977.
36. G. A. El-Shobaky, G. A. Fagal, M. Mokhtar, *Appl. Catal. A*., 1997, **155**, 167-178.

37. D. B. Rasmussen, T. V. W. Janssens, B. Temel, T. Bligarrd, B. Hinnemann, S. Helveg, J. Sehested, *J. Catal*., 2012, **293**, 205-2011.
38. X. Li, S. S. Soon Fang, J. Teo, Y. Lim Foo, A. Borgna, M. Lin, Z. Zhong, *ACS Catal*., 2012, **2**, 360-369.
39. Q. Fu, F. Yang, X. Bao, *Acc. Chem. Res*., 2013, **46**, 8, 1692-1701.

Aknoledgments. We expressed an acknowledgment to Dr. B.Markovsky (*Department of Chemistry at Bar-Ilan University Center for Advanced Materials and Nanotechnology)* for help in the Raman spectroscopy studies. Ziyi Zhong thanks Drs. Keith Carpenter and Armando Borgna *(ICES)* for their kind support of this project.

Table of Content

Paper "Doping of ZnO into CuO phase by sonochemical approach improves the CuO-ZnO/TiO_2 catalyst for WGS reaction"

By Nina Perkas[a], Poernomo Gunawan[b], Galina Amirian[a], Zhan Wang[b], Ziyi Zhong[*b] and Aharon Gedanken[*a]

[a]*Department of Chemistry and Kanbar Laboratory for Nanomaterials at Bar-Ilan University Center for Advanced Materials and Nanotechnology;*
[b]*Institute of Chemical and Engineering Sciences, 1 Pesek Road, Jurong Island, Singapore 627833, Singapore*

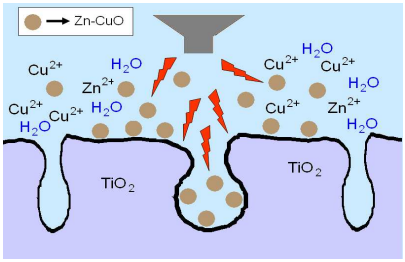

The paper reports on the CuO-ZnO/TiO_2 catalyst prepared by the ultrasound assisted method demonstrating superior activity in Water Gas Shift reaction in comparison with the catalysts synthesized by conventional incipient wetness impregnation. It is found that the sonochemical preparation offers at least two advantages: (1) generation of mesopores on the catalyst surface and (2) doping of Zn into CuO phase.

Tables and Figures

Table 1 The composition of and textual properties of catalysts and catalyst supports

Sample	Method of synthesis	Phase composition	Surface area (m^2/g)	Pore volume (cc/g)	Pore size (Å)
TiO_2 500 ^oC 3h		TiO_2: anatase + rutile	56	0.14	50
S 500	sonochemical	TiO_2: anatase + rutile CuO: tenorite	47	0.12	60
IWI 500	IWI	TiO_2: anatase + rutile CuO: tenorite ZnO: zincite	36	0.10	27
TiO_2 400 ^oC 2h		TiO_2: anatase	152	0.27	36
S 400	sonochemical	TiO_2: anatase CuO: tenorite	98	0.20	42
IWI 400	IWI	TiO_2: anatase CuO: tenorite ZnO: zincite	45	0.14	18
TiO_2 Degussa P25		TiO_2: anatase + rutile	45	0.09	< 10
TiO_2 Degussa P25 sonochemically treated		TiO_2: anatase + rutile	52	0.23	86
DS	sonochemical	TiO_2: anatase + rutile CuO: tenorite	49	0.18	74

Table 2 Elemental molar ratio in the S500, DS and IWI500 catalysts determined by EDX analysis.

Elemental molar ratio	S500	DS	IWI500
Cu/Zn	8.0	7.7	3.0
(Cu+Zn)/Ti	2.7	2.6	2.8
Cu/Ti	2.4	2.3	2.1

Figure captions.

Fig. 1 CO conversion in the WGS reaction over CuO-ZnO-TiO_2 catalysts prepared by the sonochemical and IWI methods.

Fig. 2. Life test of S500 and DS in WGS reaction at 300^{o}C.

Fig. 3 XRD patterns of the CuO-ZnO-TiO_2 catalysts prepared by sonochemical method (S500; S400) and IWI method (IWI500; IWI400) in comparison with the TiO_2 supports (TiO_2 500 and TiO_2 400). The labeling matches to the crystalline phases: A – TiO_2 anatase; R - TiO_2 rutile; T - CuO tenorite; Z – ZnO zincite, respectively).

Fig. 4 EDX results the CuO-ZnO-TiO_2 catalysts prepared by sonochemical (S500, DS) and incipient wetness impregnation (IWI500) methods.

Fig. 5 HR TEM images of CuO-ZnO/TiO_2 catalyst (S500) prepared by sonochemical method (a and b - as prepared; c and d - after catalytic reaction; e and f - after stability test at 300 ^{o}C for 90 h).
TiO_2 Anatase (101) : 0.352 nm (JCPDS no. 00-021-1272); TiO_2 Rutile (110) : 0.322 nm (JCPDS no. 00-021-1276); CuO Tenorite (002): 0.253 nm (JCPDS no. 00-041-0254).

Fig. 6. TEM images of CuO-ZnO/TiO_2 catalyst (DS) after the 90h stability test at various magnifications. The interplanar spacings and the referred JCPDS cards are:
TiO_2 Anatase (101): 0.352 nm (JCPDS no. 00-021-1272); CuO Tenorite (002): 0.253 nm (JCPDS no. 00-041-0254).

Fig. 7 Adsorption-desorption isotherms of the CuO-ZnO/TiO_2 catalysts in comparison with those of the TiO_2 supports.

Fig. 8 Schematic illustration of the formation of the CuO-ZnO/TiO_2 catalyst by the sonochemical method.

Fig. 9 Raman spectra of CuO-ZnO/TiO_2 catalysts compared to the TiO_2 support.

Fig. 10 TPR profiles of the studied catalysts and the corresponding metal oxides.

Fig. 11. Cu2p XPS spectra of the sonochemically prepared S500 and DS catalysts.

Fig.12. The microstructure of the DS catalyst after H_2-reduction.

Fig.1

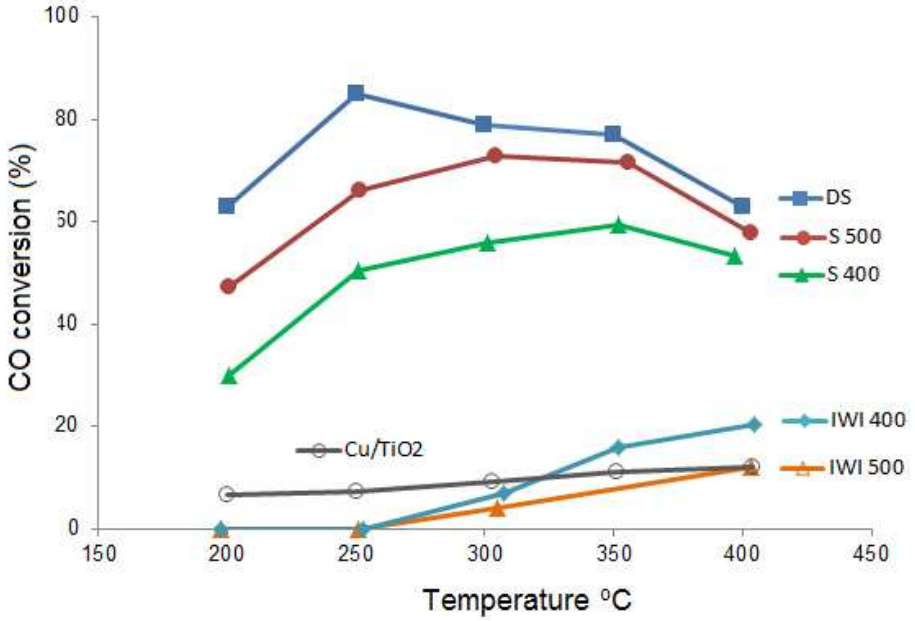

Fig.2

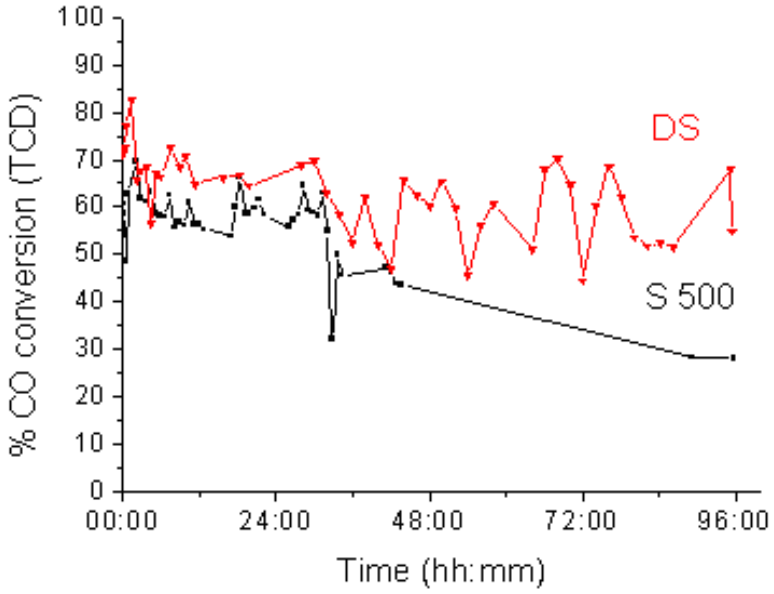

Fig. 3

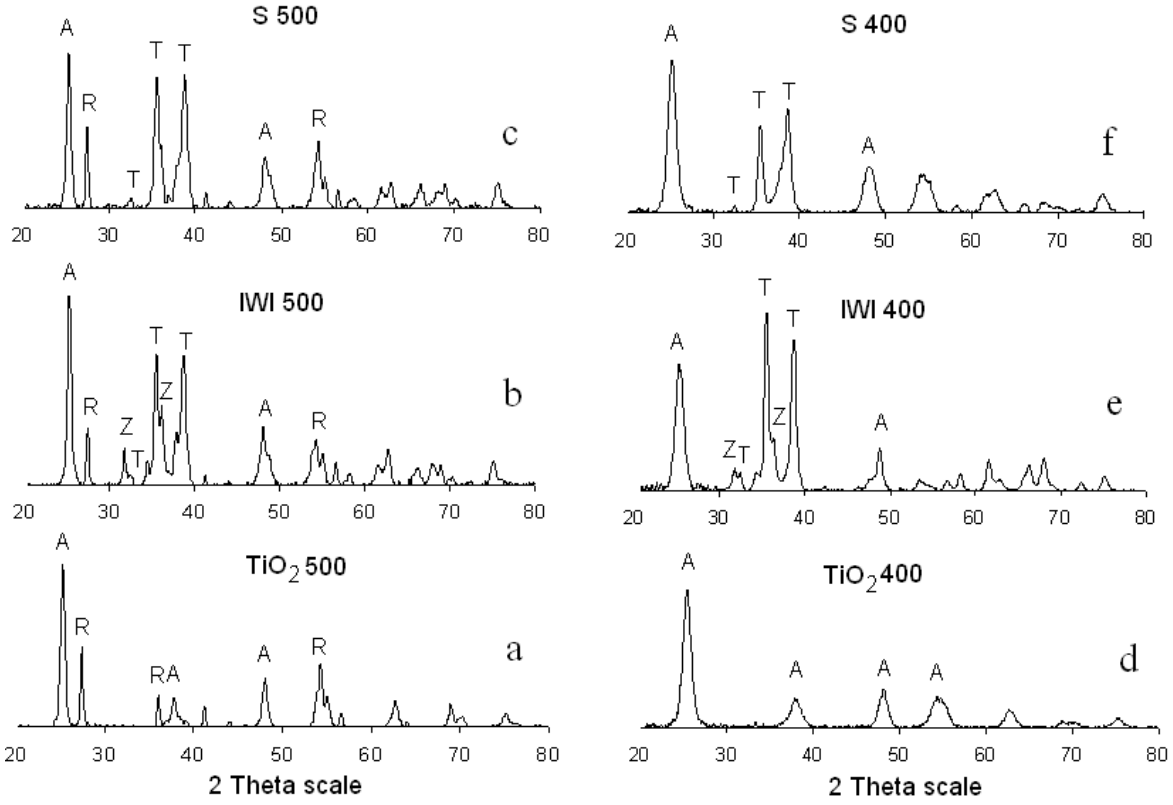

Fig. 4

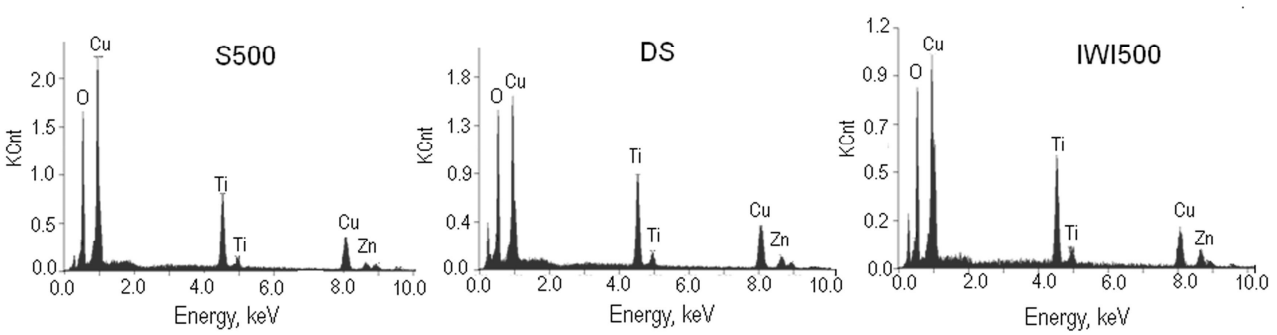

Element	*Wt%*	*At%*
OK	30.83	62.35
TiK	15.08	10.17
CuK	47.94	24.43
ZnK	06.15	3.05
Matrix	Correction	ZAF

Element	*Wt%*	*At%*
OK	29.98	61.37
TiK	15.76	10.75
CuK	47.85	24.67
ZnK	06.41	3.21
Matrix	Correction	ZAF

Element	*Wt%*	*At%*
OK	25.76	56.42
TiK	15.80	11.55
CuK	43.50	24.02
ZnK	14.94	8.01
Matrix	Correction	ZAF

Fig. 5

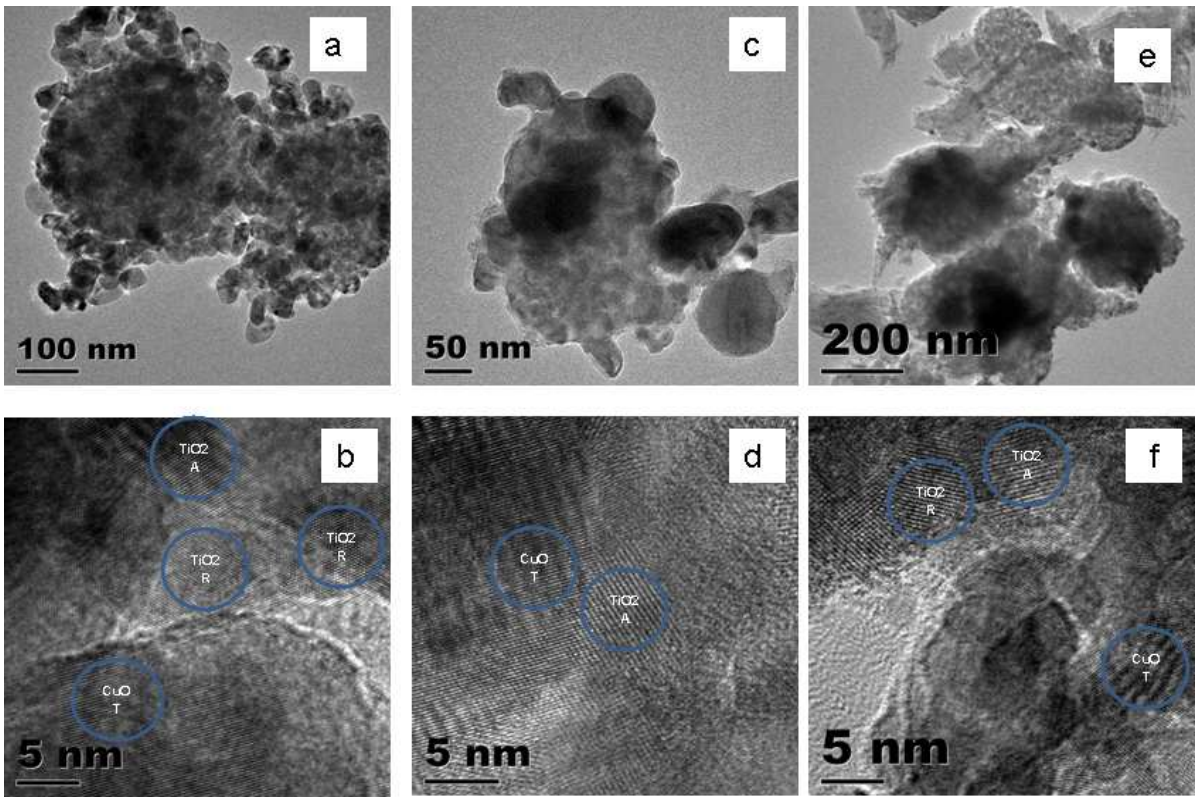

Fig.6

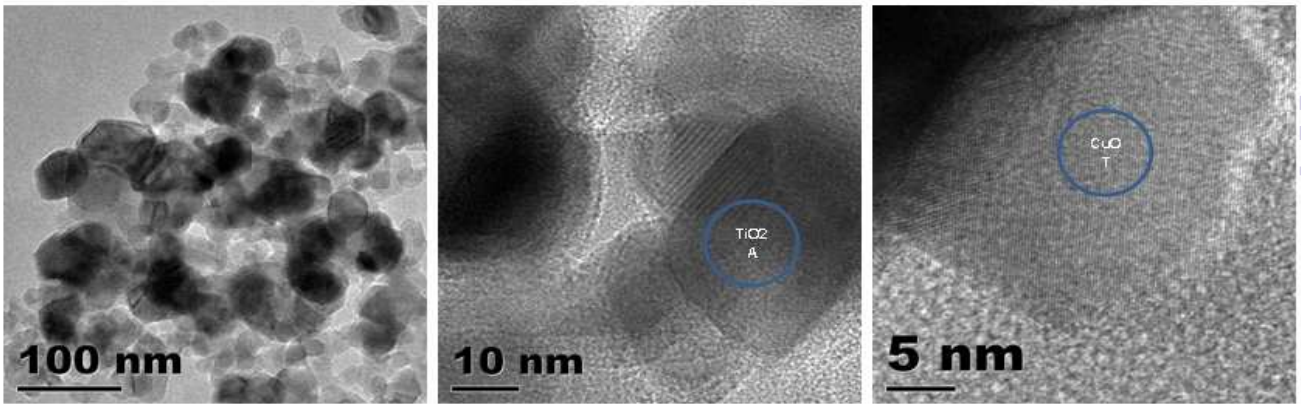

Fig. 7

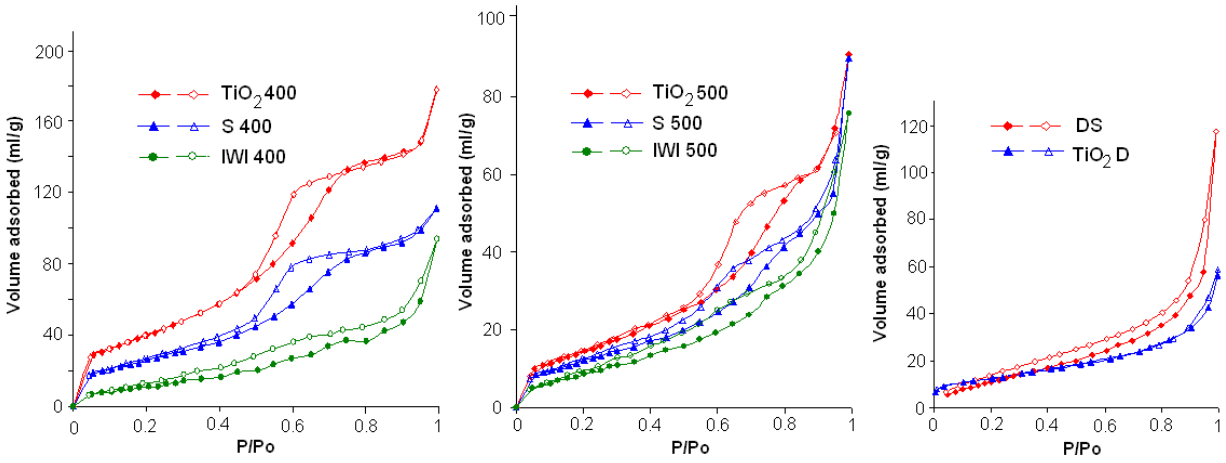

Fig. 8

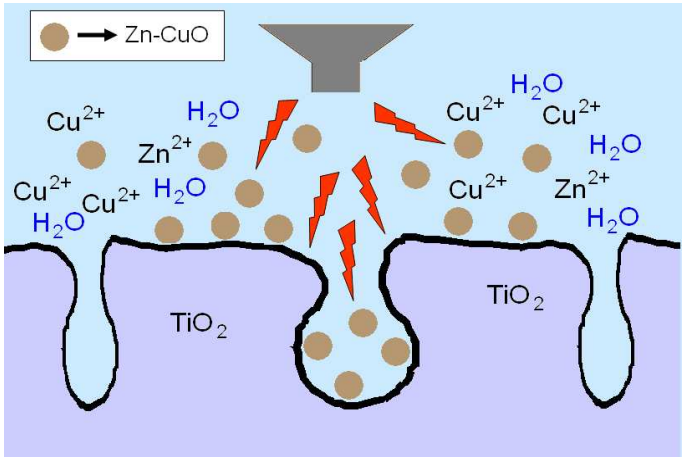

Fig. 9

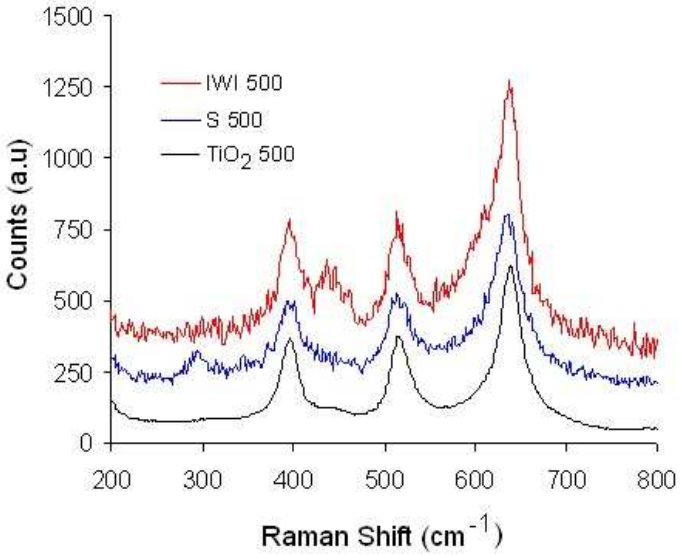

Fig. 10

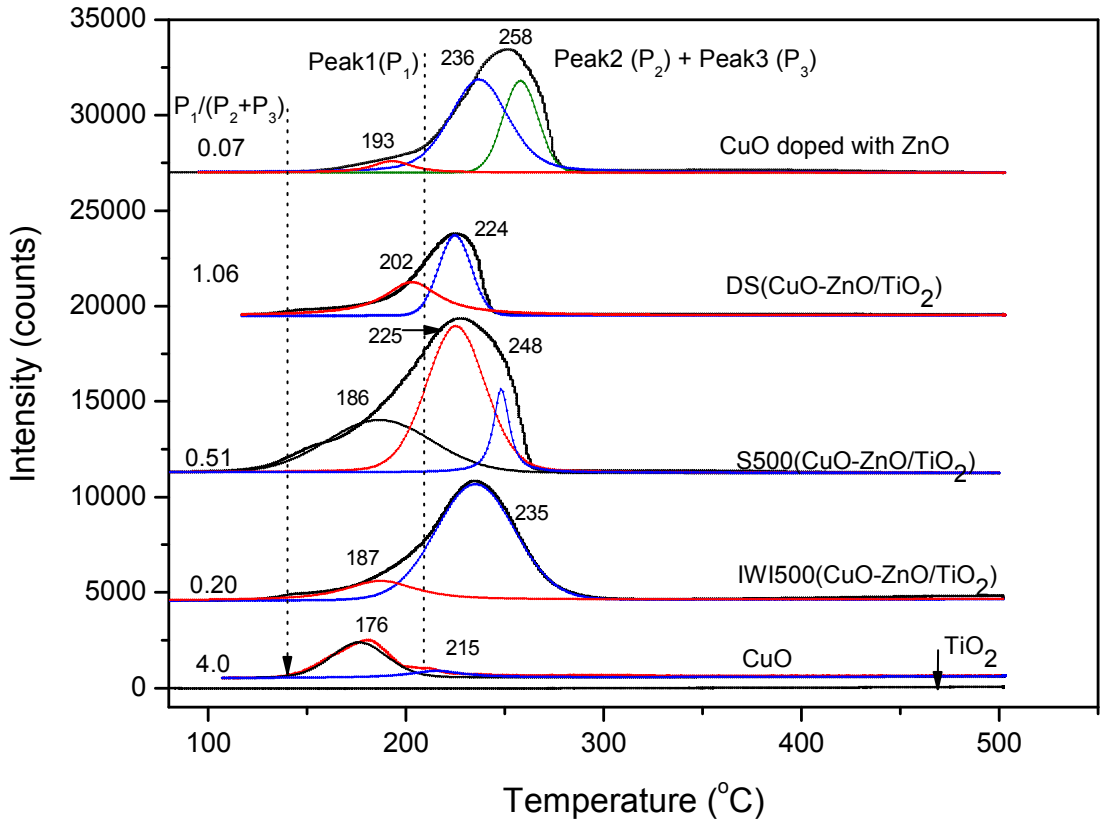

Fig. 11

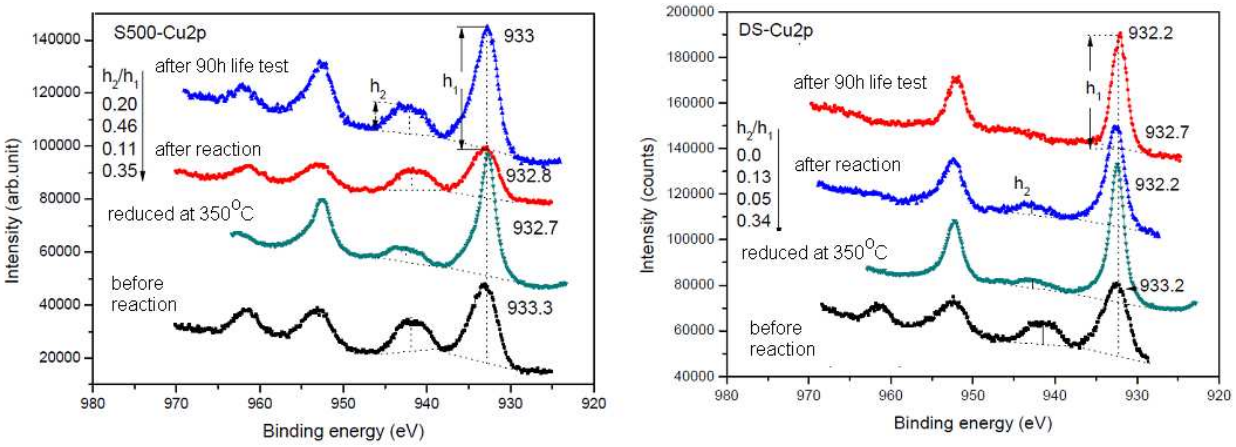

Fig.12.